



1 **Global simulations of monoterpene-derived peroxy radical fates and the distributions of highly**
2 **oxygenated organic molecules (HOM) and accretion products**

3
4 Ruochong Xu^{1,2,3}, Joel A. Thornton^{1*}, Ben H. Lee¹, Yanxu Zhang², Lyatt Jaeglé¹, Felipe
5 Lopez-Hilfiker^{1,4}, Pekka Rantala⁵, Tuukka Petäjä⁵

6
7 ¹ Department of Atmospheric Sciences, University of Washington, Seattle, WA USA 91895

8 ² School of Atmospheric Sciences, Nanjing University, Nanjing 210023, China

9 ³ Now at Department of Earth System Science, Tsinghua University, Beijing 100084, China

10 ⁴ Now at Tofwerk AG, Thun Switzerland

11 ⁵ Institute for Atmospheric and Earth System Research (INAR), University of Helsinki, Helsinki
12 00014, Finland

13
14 *To whom correspondence should be addressed: joelt@uw.edu

15
16
17 **Abstract**

18 We evaluate monoterpene-derived peroxy radical (MT-RO₂) unimolecular autoxidation and
19 self and cross reactions with other RO₂ in the GEOS-Chem global chemical transport model.
20 Formation of associated highly oxygenated organic molecule (HOM) and accretion products
21 are tracked in competition with other bimolecular reactions. Autoxidation is the dominant
22 fate up to 6-8 km for first-generation MT-RO₂ which can undergo unimolecular H-shifts.
23 Reaction with NO can be a more common fate for H-shift rate constants < 0.1 s⁻¹ or at
24 altitudes higher than 8 km due to the imposed Arrhenius temperature dependence of
25 unimolecular H-shifts. For MT-derived HOM-RO₂, generated by multi-step autoxidation of
26 first-generation MT-RO₂, reaction with other RO₂ is predicted to be the major fate
27 throughout most of the boreal and tropical forested regions, while reaction with NO
28 dominates in temperate and subtropical forests of the Northern Hemisphere. The newly
29 added reactions result in ~4% global average decrease of HO₂ and RO₂ mainly due to faster
30 self-/cross-reactions of MT-RO₂, but the impact upon HO₂/OH/NO_x abundances is only
31 important in the planetary boundary layer (PBL) over portions of tropical forests. Within the
32 bounds of formation kinetics and HOM photochemical lifetime constraints from laboratory
33 studies, predicted HOM concentrations in MT-rich regions and seasons reach 10% or even
34 exceed total organic aerosol as predicted by the standard GEOS-Chem model. Comparisons
35 to observations reveal large uncertainties remain for key reaction parameters and processes,
36 especially the photochemical lifetime of HOM and associated accretion products. Using the
37 highest reported yields and H-shift rate constants of MT-RO₂ that undergo autoxidation,
38 HOM concentrations tend to exceed the limited set of observations. Similarly, we infer that
39 RO₂ cross reactions rate constants near the gas-kinetic limit with accretion product branching
40 greater than ~0.25 are inconsistent with total organic aerosol unless there is rapid
41 decomposition of accretion products, the accretion products have saturation vapor
42 concentrations >> 1 μg m⁻³, or modeled MT emission rates are overestimated. This work
43 suggests further observations and laboratory studies related to MT-RO₂ derived HOM and
44 gas-phase accretion product formation kinetics, and especially their atmospheric fate, such



45 as gas-particle partitioning, multi-phase chemistry, and net SOA formation, are needed.

46

47 1. Introduction

48 Monoterpenes are emitted by terrestrial vegetation at a rate of approximately 50 to 100
49 Tg/yr (Arneth et al., 2008; Guenther et al., 2012; Messina et al., 2016), and are a significant
50 component of volatile consumer products (VCP) (McDonald et al., 2018). Reaction of the
51 more common monoterpenes, such as α - and β -pinene, Δ -3 carene, and limonene with
52 atmospheric oxidants is rapid, on the timescale of an hour, and produces a suite of semi-, low,
53 and extremely low volatility products which contribute to the nucleation and growth of
54 aerosol particles through the formation of secondary organic aerosol (SOA) (Bianchi et al.,
55 2019; Ehn et al., 2014; Hallquist et al., 2009; Kulmala et al., 2014; Palen et al., 1992; Pandis et
56 al., 1992; Zhang et al., 1992). Recent work has shown that even in some isoprene-dominated
57 forested regions, monoterpene oxidation products can be the major component of fine
58 particulate (PM_{2.5}) SOA mass (Lee et al., 2020; Xu et al., 2018; Zhang et al., 2018).

59

60 Laboratory studies have shown that at least 30 to 50% of the condensable mass produced
61 during oxidation of α -pinene, by both the hydroxyl radical (OH) and ozone, is formed
62 promptly in the first generation of oxidation (Berndt et al., 2016; Ehn et al., 2014; Jokinen et
63 al., 2015; Mentel et al., 2015). This prompt formation of low volatility mass stems from a
64 fraction of the first-generation organic peroxy radicals (RO₂) undergoing repeated
65 unimolecular H-shift reactions followed by O₂ addition, ultimately leading to Highly
66 Oxygenated-organic Molecules (HOM) which are low or even extremely low volatility. The
67 unimolecular H-shifts are the rate-limiting steps to HOM formation, and have been shown
68 for certain RO₂ to exceed 1 s⁻¹ at ~296 K (Xu et al., 2019). At such timescales, bimolecular
69 reactions of RO₂ with the hydroperoxy radical (HO₂), other RO₂, and nitric oxide (NO), even if
70 the latter is present at up to 1 ppb, are not competitive, and autoxidation to HOM is
71 expected to be a dominant fate for such RO₂ in the atmosphere. Moreover, the rate
72 constants of corresponding RO₂ cross-reactions, and the branching to accretion products,
73 presumably organic peroxides (ROOR'), have been shown to be substantially larger than
74 previous expectations (Berndt et al., 2018a, 2018b) and important to new particle formation
75 and growth (Bianchi et al., 2019). The ROOR' products can be of low or extremely low
76 volatility as well, even without substantial RO₂ H-shift chemistry, but cross reactions between
77 isoprene-derived RO₂ and MT-HOM RO₂ specifically can be important in limiting ELVOC
78 formation and thus nucleation (McFiggans et al., 2019).

79

80 Relatively few studies to date have evaluated the global implications of such revisions to our
81 understanding of monoterpene (MT) RO₂ fate (Jokinen et al., 2015; Weber et al., 2020).
82 Jokinen et al. (2015) showed the impact of MT-HOM formation at specified yields on SOA
83 budgets and CCN. Weber et al (2020) use a condensed reaction mechanism to more explicitly
84 treat the formation of HOM through unimolecular MT-RO₂ autoxidation and cross reactions.
85 However, global-scale simulations with online MT-RO₂ chemistry and comparisons to
86 observations, either using total organic aerosol mass as a constraint or more specific
87 molecular composition measurements of gas and aerosol phase species, remain lacking.
88 Moreover, the sensitivity of HO_x, O₃, and NO_x abundances and lifetimes to such changes in



89 RO₂ chemistry have yet to be fully explored in global chemical transport models. The
90 unimolecular MT-RO₂ chemistry and faster RO₂ cross reactions have implications for HO_x
91 partitioning, OH recycling, and NO_x lifetime in low-NO_x forested regions. In addition,
92 measurements of highly oxygenated organic nitrates can provide insights into the MT-RO₂
93 reactivity governing the competitions between autoxidation, RO₂ cross reactions, and RO₂
94 reactions with nitric oxide (NO).

95
96 Herein, we use the GEOS-Chem global chemical transport model to evaluate the impact of
97 MT-RO₂ H-shift and cross-reactions on tropospheric Hydrogen oxide radicals (HO_x = OH + HO₂)
98 and total RO₂ abundance, ozone distributions, and assess the potential contribution of MT-HOM
99 and HOM-nitrates to low and extremely low volatility components and by extension the global
100 budget of SOA. We update the GEOS-Chem mechanisms for MT oxidation, using where possible
101 laboratory-derived values of mechanistic parameters, such as MT-RO₂ unimolecular H-shift rate
102 constants, the fraction of MT-RO₂ undergoing H-shifts, and the rate constants for cross-reactions
103 between MT-RO₂ and other RO₂, such as those derived from isoprene oxidation. We compare
104 predicted HOM and HOM-nitrates to atmospheric observations in the gas and particle phases
105 from two locations and conduct sensitivity studies to evaluate the impacts of uncertain kinetic
106 parameters and mechanistic assumptions.

107

108 2. Methods

109 2.1 GEOS-Chem Model

110 We use the GEOS-Chem chemical transport model (Bey et al., 2001) which is driven by
111 assimilated meteorological fields from the MERRA-2 (Modern-Era Retrospective analysis for
112 Research and Applications, Version 2) (Gelaro et al., 2017). Simulations were conducted with
113 2°×2.5° LAT × LON horizontal resolution and 47 vertical levels for 28 months from March
114 2012 to June 2014. This time period provides the best overlap with available observations of
115 monoterpene-derived oxidation products in gas and particle phases made during the SOAS
116 and BAECC field campaigns, described in detail elsewhere (Carlton et al., 2018; Lee et al.,
117 2016, 2018; Lopez-Hilfiker et al., 2016; Petaja et al., 2016), and discussed further below. The
118 first year of the simulation was for spin-up purposes, to allow for accumulation of
119 intermediate chemical reservoir species. For comparison to the observations, we sample the
120 model in time and space corresponding to lowest model grid box containing the location of
121 the observations.

122

123 A reference simulation was conducted based on the public version 12.1.0 of GEOS-Chem
124 (link). The HO_x-NO_x-VOC-O₃-BrO_x tropospheric chemistry chemical mechanism in the
125 reference simulation is described in Mao et al., (2010, 2013) with recent updates for biogenic
126 VOC chemistry (Fisher et al., 2016; Travis et al., 2016). Emissions of isoprene and
127 monoterpenes are driven by the Model of Emissions of Gases and Aerosols from Nature v2.1
128 (MEGAN, Guenther et al., 2012). Emissions in GEOS-Chem are based on the Harvard-NASA
129 Emission Component (HEMCO) (Keller et al., 2014). Global anthropogenic emissions of NO_x,
130 SO₂, CO and various aerosol species are from the CEDS (Community Emission Data System)
131 combined with MIX in Asia, NEI in USA, APEI in Canada, BRAVO in Mexico, EMEP in Europe
132 and DICE in Africa. Open fire emissions are from Global Fire Emissions Database (GFED4).



133 Both gas and aerosol are dry-deposited, with rates calculated online based on the
134 resistance-in-series algorithm (Wesely, 1989; Zhang et al., 2001). Wet deposition is calculated
135 for water-soluble aerosol and gas following (Amos et al., 2012; Liu et al., 2001).

136

137 **2.2 Updates to the GEOS-Chem MT Oxidation Mechanism**

138 Our goal for the mechanism updates was to preserve as much as possible the current
139 simplified framework for MT chemistry in GEOS-Chem, but to include the essential features
140 of MT-RO₂ unimolecular H-shift and bimolecular RO₂ cross-reactions (see Figure 1). Thus, RO₂
141 and closed-shell products become quickly lumped into corresponding pools that loosely
142 relate to the dominant functional group character, such as carbonyl, alcohol, nitrate, etc. In
143 this version, we restricted changes to chemistry stemming from OH reaction and ozonolysis
144 only, we do not consider nitrate radical (NO₃) reactions of MT. In what follows, to maintain a
145 higher level of clarity, we mostly discuss the mechanism in general terms. Values of
146 mechanistic parameters can be found in Table S1-S5 and are discussed in more detail in the
147 online supplemental information (SI).

148

149 To account for MT-RO₂ H-shift chemistry leading to HOM (i.e. “autoxidation”), we split the
150 first-generation MT-RO₂ formed from the reaction of MT with OH or ozone, into two pools,
151 either MT-aRO₂ or MT-bRO₂. Both types of RO₂ undergo the usual bi-molecular reactions, but
152 MT-aRO₂ do not undergo unimolecular H-shift, while MT-bRO₂ do. The branching between
153 MT-aRO₂ or MT-bRO₂ from MT + OH or MT + O₃ reactions are based on laboratory-derived
154 yields of MT-HOM and MT-nitrates, which typically find that the fraction of MT-RO₂
155 undergoing autoxidation is <0.5 (Berndt et al., 2016; Kurten et al., 2015; Richters et al., 2016)
156 but can be higher in some studies (Xu et al., 2019). The competitive yields of MT-HOM will
157 be sensitive to the multiplicative product of H-shift rate constant and this fraction. As a result,
158 we vary this fraction for both OH and O₃ reactions as part of sensitivity studies. While
159 MT-aRO₂ do not undergo unimolecular H-shift, we allow for a small fraction of MT-aRO₂
160 reactions involving NO or NO₃ to produce MT-bRO₂ to simulate the corresponding alkoxy
161 radicals undergoing opening of the 4-member ring which is often part of first-generation RO₂
162 formed from α -Pinene ozonolysis and OH reactions. Opening of the 4-member ring would
163 lead to RO₂ structures more amenable to unimolecular H-shift reactions (Iyer et al., 2021;
164 Kurten et al., 2015).

165

166 The fraction of first-generation MT-RO₂ able to undergo unimolecular H-shifts, and thus
167 autoxidation (MT-bRO₂), is 20% from MT + OH and 3% from MT + O₃, in the base simulation
168 (Table S3). A single temperature-dependent rate constant, k_{Hshift} , based upon recent
169 laboratory studies and quantum chemical calculation of associated energy barriers is used to
170 describe these H-shifts. We use an activation energy of 17.7 kcal/mol based on the
171 calculations in Berndt et al., (2016). Two values of k_{Hshift} , near 1.0 s⁻¹ and 0.1 s⁻¹ at 298K, are
172 tested in sensitivity studies. The H-shift reactions of MT-bRO₂ are assumed to be followed by
173 O₂ addition to form a new peroxy radical, MT-cRO₂, which in turn can also continue
174 autoxidation to form a yet more oxidized MT-HOM-RO₂. This sequence of RO₂ autoxidation,
175 occurring in competition with typical bimolecular reactions, simulates a first generation of
176 MT-RO₂, C₁₀H₁₅O₄ or C₁₀H₁₇O₃, undergoing two H-shift/O₂ addition steps to form RO₂ with



177 compositions of $C_{10}H_{15}O_8$ or $C_{10}H_{17}O_7$, respectively, that are consistent with the current
178 definition of HOM (Bianchi et al., 2019).

179

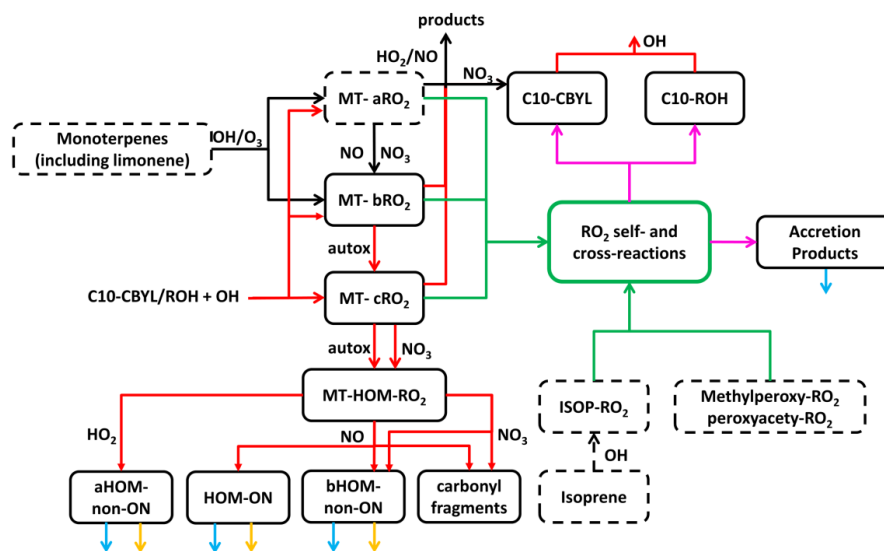
180 These MT-HOM-RO₂ undergo only bimolecular reactions with HO₂, RO₂, and NO₂, NO₃.
181 Except for RO₂ cross-reactions, discussed further below, rate constants for such reactions are
182 the default values used in GEOS-Chem for other RO₂. The products of these reactions are
183 split into four categories, three of which are HOM. Reaction of MT-HOM-RO₂ with HO₂ is
184 assumed to produce only HOM monomers (aHOM) without a nitrate group. Reaction with
185 NO leads to HOM organic nitrates (HOM-ON), a second class of HOM without a nitrate group
186 (bHOM), and hydroxy carbonyl fragments assumed to be C₅ species. The branching ratio for
187 HOM-ON formation is assumed to be 0.2, determined using typical literature
188 parameterizations based on the carbon number. We explicitly distinguish between
189 non-nitrate HOM that result from reaction of MT-HOM-RO₂ with HO₂ (aHOM) or NO (bHOM)
190 to allow for better accounting of RO₂ fate and the specific impact of NO on HOM. The
191 assumption that the alkoxy radical formation channel of MT-HOM-RO₂ reactions with NO
192 leads to HOM is not well constrained, but it is typically a minor component of the HOM yield
193 on a global average. We neglect further autoxidation reactions of RO₂ and alkoxy radicals,
194 and some of the fragmentation channels of the resulting alkoxy radicals may well produce C₉
195 or C₈ products that still meet the HOM definition. Reaction of MT-HOM-RO₂ with the nitrate
196 radical (NO₃) is assumed to produce only an alkoxy radical product (and NO₂), and the alkoxy
197 radical either forms a bHOM (non-nitrate), similar to that from reaction of the RO₂ with NO,
198 or a C₅ hydroxy carbonyl product to represent fragmentation into non-HOM products. We
199 assume equal branching for these two pathways, which might lead to a slight overestimate
200 of MT-HOM, but reaction with NO₃ is a typically a minor fate for MT-HOM-RO₂.

201

202 After addition of RO₂ H-shift chemistry, the next most significant change to monoterpene
203 chemistry we incorporated into GEOS-Chem involves the self- and cross-reactions of RO₂. We
204 specifically evaluated the impact of a higher rate constant and allowed for accretion product
205 formation in competition to the more common alkoxy radical and disproportionation
206 channels which lead to lumped carbonyl (C₁₀-CBYL) and alcohol (C₁₀-OH) products following
207 the typical lumping strategy in GEOS-Chem. Our basis for these changes includes the recent
208 laboratory studies described in Berndt et al., (2018a, 2018b) and Zhao et al., (2018), where
209 cross-reaction rate constants were found to range from 10⁻¹² to 10⁻¹⁰ cm³ molec⁻¹ s⁻¹ and
210 accretion product branching ranged from 4 to >50%. Given that there are only self-reactions
211 for isoprene-derived RO₂ in the current GEOS-Chem without branching to accretion products,
212 taking even the lower range from laboratory studies would represent a major shift in RO₂
213 fate. Important for regions with intense biogenic VOC emissions and relatively low NO_x (such
214 as regions of the Amazon), we specifically include cross-reactions between monoterpene and
215 isoprene derived RO₂. Our simulations include both low and high estimates of RO₂ self- and
216 cross-reaction rate constants to better demonstrate the range of possible impacts of these
217 reactions, and we also apply different rate constants for highly oxidized RO₂ (Table S4). For
218 the rate constants considered, RO₂ cross reactions can become competitive or even
219 dominant fates of RO₂ and thus impact the abundance and recycling of HO_x as well as the
220 formation of low volatility products that would contribute to organic aerosol. For accretion



221 products, we use a conservative branching (4%) from self- and cross-reactions to produce
 222 C20 or C15 compounds, except for HOM-RO₂ self and cross reactions, for which we also
 223 examine a unit branching to accretion products as suggested by some laboratory studies
 224 (Berndt et al., 2018a, 2018b).
 225



226
 227 **Figure 1.** The main reactions and processes included in the updated scheme are shown.
 228 Chemical species in solid boxes are newly added while those in dashed boxes already exist in
 229 the GEOS-Chem mechanism. Dashed-line black arrows represent originally existing reactions
 230 without any modification, and solid black arrows represent those with certain modifications
 231 in the scheme. Red, green, and magenta arrows represent newly-added RO₂ formation and
 232 loss. Blue and yellow arrows represent dry-/wet-deposition and photolysis, respectively.
 233 More details are shown in SI.

234
 235 The fate of MT-HOM we assume is dominated by deposition (wet and dry) or by photolysis.
 236 While reaction with OH or other radical oxidants is possible, our assumption is that the vast
 237 majority of HOM produced in this mechanism will be of low or extremely low volatility and
 238 thus be present predominantly in submicron aerosol particles. As we do not explicitly
 239 consider gas-particle partitioning in this version, we therefore use a single photolysis
 240 frequency equal to 1/60 of j_{NO_2} to account for photochemical degradation of particle-phase
 241 HOM. While we do not treat heterogeneous oxidation explicitly, we assume our photolysis
 242 parameterization accounts for this process. The value of the photolysis frequency is based on
 243 how well the model reproduces HOM observations in the absence of further photochemical
 244 degradation, and also on laboratory chamber experiments showing loss of HOM and
 245 associated MTSOA mass over time (Krapf et al., 2016; Pospisilova et al., 2020; Zawadowicz et
 246 al., 2020). The photochemical fate of HOM remains one of the most uncertain aspects of the
 247 mechanism. We parameterize HOM wet deposition following aerosol-phase organic nitrate
 248 in (Fisher et al., 2016), and dry deposition is calculated online based on the



283 Brazil were used for comparisons (Carlton et al., 2018; Martin et al., 2016; Petaja et al., 2016).
284 Measurements of organic aerosol mass concentrations from aerosol mass spectrometer
285 (AMS) instruments (DeCarlo et al., 2006; Jayne et al., 2000) and gas- and particle-phase HOM
286 from High-Resolution Time of Flight Chemical Ionization Mass Spectrometers (HRToF-CIMS)
287 were used when available (Lopez-Hilfiker et al., 2014). For HOM measurements, molecular
288 formulas of compounds contain 10 carbon atoms and greater than or equal to 7 oxygen
289 atoms were selected as HOM for comparisons. Those with one nitrate atom and without
290 nitrate were compared to simulated HOM-ON and HOM-non-ON, respectively. We also
291 compared predicted HOM to total organic aerosol mass (OA) from aerosol mass
292 spectrometer measurements assuming HOM was present predominantly in submicron
293 aerosol particles. Besides HOM, closely related species in the scheme were also compared
294 when available, including NO, O₃, monoterpenes and isoprene. The details on the
295 measurements were presented in SI including top contributing HOM species identified in
296 data from SENEX and BAECC (Table S7 and S8).
297

298 3. Results and discussion

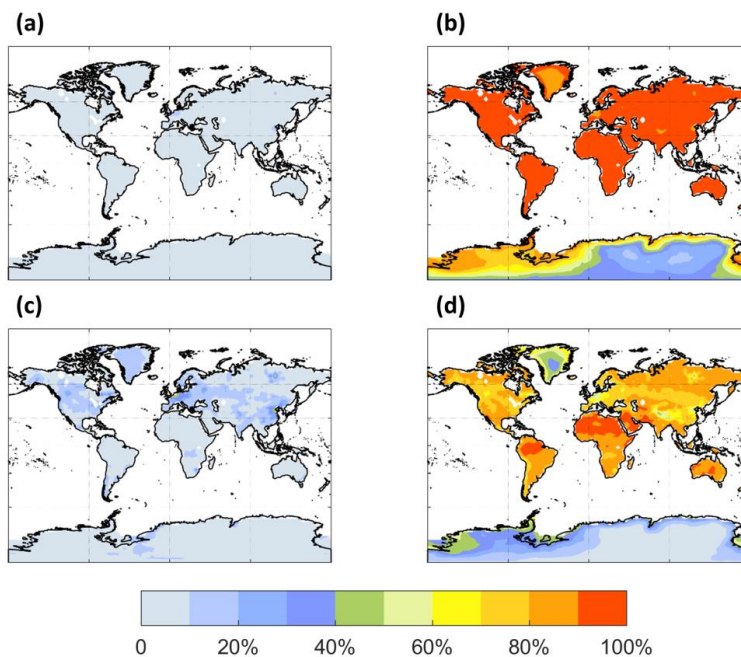
299 3.1 MT and HOM RO₂ Fates

300 The largest change to the current mechanism was to the fate of a fraction of MT-derived RO₂,
301 where we incorporated unimolecular autoxidation reactions for a subset of first-generation
302 MT-derived RO₂ (MT-bRO₂ in the above scheme), as well as enhanced reaction rate constants
303 for bimolecular RO₂ self and cross reactions between MT and isoprene RO₂. The fate of RO₂
304 determines the volatility and reactivity of HOM and thus of the potential for HOM
305 contribution to aerosol formation and growth. In our simplified treatment, we assume
306 HOM-RO₂ only undergo bimolecular reactions. HOM-RO₂ that undergo unimolecular
307 decomposition to a closed-shell product, such as by OH or HO₂ elimination, may result in a
308 non-HOM product. Thus, our flux of MT to HOM-RO₂ may be underestimated, but net HOM
309 production may be more accurate.
310

311 The spatial distribution of the annual average reaction fate of MT-bRO₂ in the planetary
312 boundary layer (PBL) is shown in Figure 2 for two simulation cases, LowProd_Photo (panels
313 a-b) and LowProd_Photo_kauto_Slow (panels c-d). The difference between these two
314 simulations is the rate constant for the unimolecular RO₂ H-shift (~1.0s⁻¹ vs. ~0.1s⁻¹ at 298K,
315 respectively). For either case, unimolecular H-shift and subsequent autoxidation is the
316 dominant fate of the first-generation MT-bRO₂ throughout the PBL on average. While likely
317 dependent upon model resolution, when k_{auto} is ~ 0.1 s⁻¹, the reaction with NO becomes a
318 more common fate for MT-bRO₂, but never more than 50% of the total fate of this HOM-RO₂
319 precursor, even in NO_x-polluted regions such as the SE U.S., eastern China, and Western
320 Europe. In Figure 3, the annually averaged vertical profiles of MT-bRO₂ fate are shown for
321 two model grid points, one containing Centreville, AL and the other in the Amazon
322 containing the T3 site of the Go-Amazon campaign. The dominance of unimolecular RO₂
323 H-shift and autoxidation as a fate for MT-bRO₂ persists up to 6 to 8 km, even though its rate
324 is decreasing exponentially with decreasing temperature. In both locations, reaction with NO
325 at high altitudes becomes a major MT-bRO₂ fate, especially over the SE U.S., while over the
326 Amazon reaction with HO₂ and NO above 6 km are of similar importance likely reflecting the



327 combination of the activation energy required for the unimolecular H-shift, decreases in
328 temperature with altitude, and NO in the upper troposphere from lightning and convection.
329



330

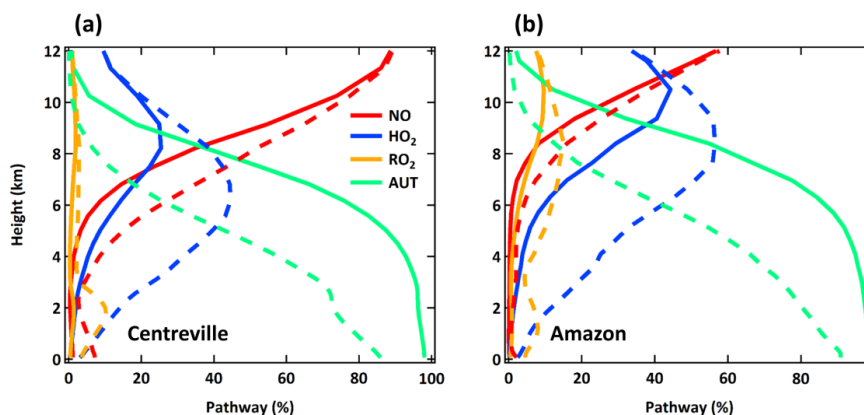
331 **Figure 2.** The annually PBL-averaged MT-bRO₂ consumption fractions by NO (left panel) and
332 autoxidation (right panel) from experiments LowProd_Photo (a)-(b) and
333 LowProd_Photo_kauto_Slow (c)-(d). Autoxidation rate constant is $\sim 1.0 \text{ s}^{-1}$ and $\sim 0.1 \text{ s}^{-1}$ at
334 298K in two experiments, respectively. The fractions by HO₂, NO₃ and RO₂ are shown in
335 Figure S1.

336

337 **Table 2.** Global PBL-average MT-bRO₂ fates weighted by gridded MT-bRO₂ concentrations on
338 land.

| | LowProd_Photo | LowProd_Photo_kauto_Slow | |
|---------------------|-----------------|--------------------------|------------------|
| MT-bRO ₂ | Autoxidation | 93% | 77% |
| | NO | 1% | 6% |
| | HO ₂ | 6% | 16% |
| | RO ₂ | $\sim 10^{-4}\%$ | $\sim 10^{-3}\%$ |
| | NO ₃ | 0.4% | 1.6% |

339



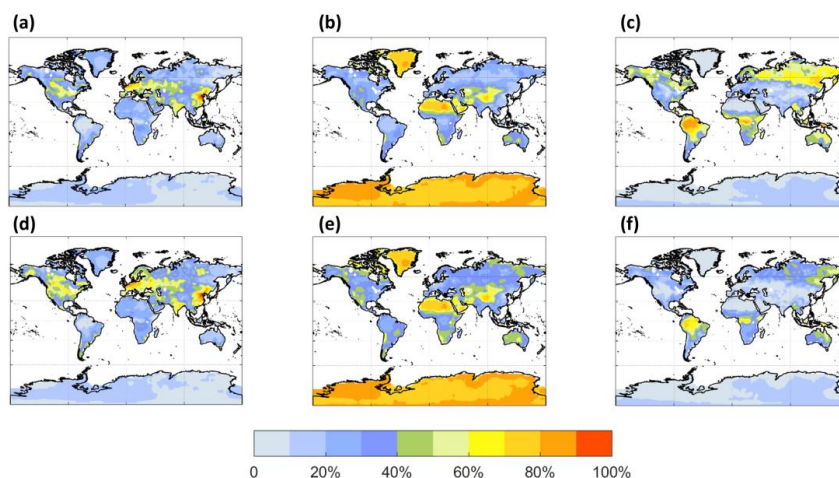
340
341 **Figure 3.** Annual averaged vertical profiles of four dominant reaction pathways of MT-bRO₂
342 at Centreville, AL USA and over the Amazon near Manaus, from simulations LowProd_Photo
343 (solid lines) and LowProd_Photo_kauto_Slow (dashed lines). Reaction with NO₃ contributes
344 less than 1% and it is thus not shown here.

345
346 Figures 4 and 5 are similar to Figures 3 and 4, but for the fates of HOM-RO₂ instead of
347 MT-bRO₂. As HOM-RO₂ in the model do not undergo unimolecular reactions (see above),
348 these fates are more similar to generic RO₂ chemistry in the model with the important
349 exception that the rate constants for self and cross-reactions between HOM-RO₂ and other
350 RO₂ are in general much larger than those typical of other RO₂ in GEOS-Chem. The case
351 where HOM-RO₂ rate constants for RO₂ cross reactions are relatively large (LowProd_Photo,
352 Figure 4 panels a-c), e.g. as in Berndt et al., (2018a), reaction with RO₂ is predicted to be the
353 dominant HOM-RO₂ fate throughout most of the boreal and tropical forest regions as well as
354 portions of the SE US. In temperate and subtropical forests of the N. Hemisphere, reaction
355 with NO is the major fate for HOM-RO₂. The potential importance of reactions with RO₂
356 being a dominant fate is two-fold. First, the branching of such reactions to accretion products
357 is uncertain (see below), but likely also critical for participation of biogenic VOC in the
358 nucleation of particles (Bianchi et al., 2019; Kulmala et al., 2014). However, the portion of
359 such reactions which do not undergo accretion otherwise can result in less carbon mass
360 moving to lower volatility due to C-C bond scission of alkoxy radical products (Orlando et al.,
361 2003). In the simulation with slower RO₂ cross-reactions (e.g. LowProd_Photo_Slow), rate
362 constants for which are near the lower limit of rate constant collections from several
363 laboratory studies (Berndt et al., 2018a, 2018b; Zhao et al., 2018), RO₂ cross reactions
364 remain important (~40%) across boreal forests, but are no longer dominant as a HOM-RO₂
365 fate except in the tropical forest regions. Reactions with NO expand in importance in boreal
366 forest regions in this simulation, at times being the dominant fate in regions of the N.
367 American boreal forest. While consistently significant, typically at 30 to 40% of HOM-RO₂ fate,
368 reaction of HOM-RO₂ with HO₂ is only rarely a majority fate in the PBL over forested regions.

369
370 The annual average HOM-RO₂ fate changes significantly between the boundary layer and
371 free troposphere as shown in Figure 5 for the same two model locations in Figure 3.



372 Throughout the low and middle troposphere in both locations, reaction with HO₂ becomes
 373 the dominant HOM-RO₂ fate in both locations, followed by RO₂ over the Amazon, and NO
 374 over the SE US. Reaction with NO becomes the dominant fate for HOM-RO₂ in the upper
 375 troposphere over the SE US, while NO, HO₂ and RO₂ reactions are predicted to be of similar
 376 importance over the Amazon.



377
 378 **Figure 4.** The annually PBL-averaged MT-HOM-RO₂ relative fates including reaction with NO
 379 (left panel), HO₂ (middle panel) and RO₂ (right panel) from simulation LowProd_Photo (a)-(c)
 380 and LowProd_Photo_Slow (d)-(f). Reaction with NO₃ contributes <1% and it is thus not
 381 shown here.

382

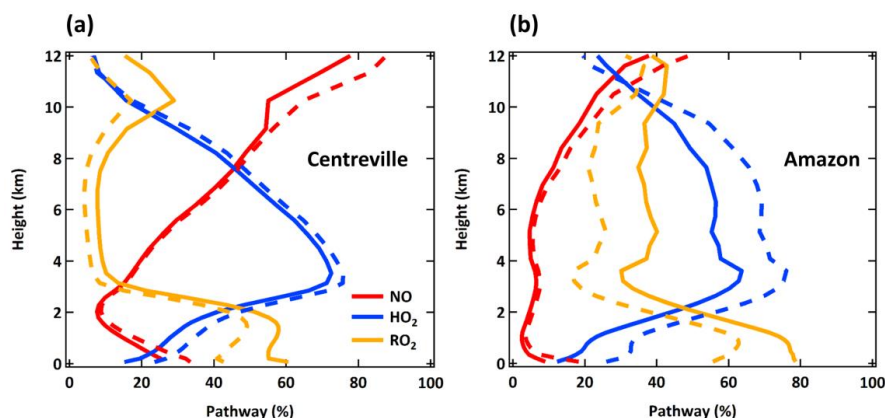
383

384

Table 3. Global PBL-average MT-HOM-RO₂ fates weighted by gridded MT-HOM-RO₂
 concentrations on land.

| | | LowProd_Photo | LowProd_Photo_Slow |
|------------------------|-----------------|---------------|--------------------|
| MT-HOM-RO ₂ | NO | 16.44% | 20.71% |
| | HO ₂ | 22.00% | 33.12% |
| | RO ₂ | 61.54% | 46.11% |
| | NO ₃ | 0.02% | 0.06% |

385



386

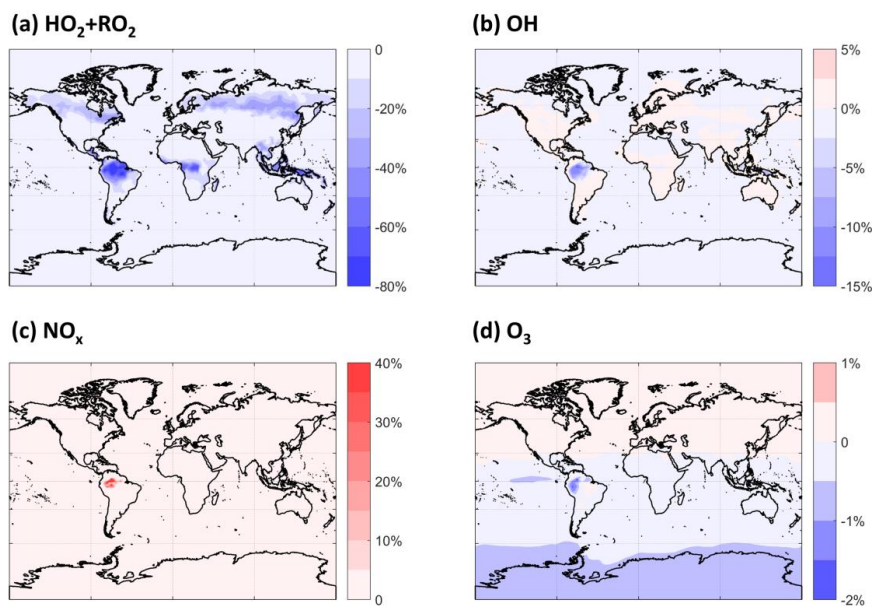
387 **Figure 5.** Annual averaged vertical profiles of three dominant reaction pathways of
388 MT-HOM-RO₂ at Centreville, AL and Amazon near Manaus, from simulation LowProd_Photo
389 (solid lines) and LowProd_Photo_Slow (dashed lines). Reaction with NO₃ contributes < 1%
390 and it is thus not shown here.

391

392 3.2 Impact on HO_x, NO_x, and O₃

393 By altering the fates of MT-derived RO₂ chemistry and the interactions thereof with
394 isoprene-derived RO₂, we expect that the cycling and lifetime of HO_x are affected. Changes in
395 HO_x abundance and distribution will alter NO_x cycling and fate, which will potentially impact
396 tropospheric O₃. MT are not typically major components of OH reactivity, even in
397 biogenically influenced regions so these impacts are not expected to be large. As shown in
398 Figure 6, there are substantial decreases in the sum of HO₂ and RO₂ concentrations in certain
399 regions averaged over the planetary boundary layer (PBL), the height of which is taken from
400 the MERRA-2 reanalysis data (Gelaro et al., 2017). HO₂ and RO₂ concentrations together
401 decrease by as much as ~20% over boreal forests and up to 80% over tropical forests. The
402 global average decrease in the sum of HO₂ and RO₂ in this simulation compared to the
403 default is 4%. The updated description of RO₂ self and cross reactions is the dominant driver
404 of the shorter RO₂ lifetime and thus of the calculated decreases. Given that most of these
405 decreases in RO₂ occur in locations with low NO, the impact upon HO₂ and OH (Figure 6b) are
406 small globally, but not negligible in the PBL over the Amazon, reaching a ~15% decrease in
407 OH. The lower OH predicted over the Amazon leads to longer NO_x lifetimes there and thus a
408 highly localized increase in NO_x abundance. Otherwise, the effects on NO_x and O₃ are
409 negligible globally.

410



411

412 **Figure 6.** The annual PBL-averaged relative differences of (a) HO₂+RO₂, (b) OH, (c) NO_x and (d)
413 O₃ between simulations LowProd_Photo and Default.

414

415

416

417

4183.3 HOM and associated accretion product distribution and concentrations

419 **Table 4.** Global annual budgets of MT-HOM and MT-RO₂ accretion products
420 from Mar. 2013 to Feb. 2014 (unit: kt C).

| | Chemistry | Wet deposition | Dry deposition |
|-----------------------------|-----------|----------------|----------------|
| HOM-non-ON | 321 | -277 | -45 |
| HOM-ON | 26 | -20 | -6 |
| Total accretion products | 2107 | -1907 | -204 |

421

422 Global annual budgets for the chemistry (Production + Loss), and wet and dry deposition of
423 HOM-non-ON, HOM-ON and MT-derived accretion products are summarized in Table 4 from
424 the LowProd_Photo_kauto_slow simulations. For even the slowest kauto used, the
425 non-nitrate pathway for HOM is more than factor of 10 that of HOM organic nitrates.
426 Interestingly, even for a small branching to accretion products, MT-RO₂ derived accretion
427 products are a substantially larger fate than HOM, suggesting either that the rates and
428 branching are too high or that the chemical loss pathways of associated products are not
429 well represented.

430

431 The PBL average mass concentrations (μg m⁻³) of HOM predicted by the model are shown in



432 Figure 7 (a-d) for the LowProd_noPhoto, which produces middle-to-upper range estimates of
433 HOM concentrations out of the other scenarios tested. Maps from other sensitivity
434 simulations are included in the SI (Figure S2-S6). In this scenario, monoterpene-derived HOM
435 are predicted to average near $1 \mu\text{g m}^{-3}$ in the PBL over tropical forests with little seasonality,
436 while in the temperate and boreal forests of N. America, Europe, and east Asia, HOM reach
437 0.5 to $1 \mu\text{g m}^{-3}$ during summer months. In the LowProd_Photo scenarios, HOM
438 concentrations average an order of magnitude lower than shown in Figure 7, though the
439 spatial and seasonal patterns are similar. Given that HOM with 10 carbons and 7 or more
440 oxygens will be low or extremely low volatility, the majority of HOM produced from
441 monoterpene oxidation will likely contribute to SOA and thus to total OA. A background
442 organic aerosol mass concentrations in rural or remote forested regions of order $1 \mu\text{g m}^{-3}$
443 outside of biomass burning periods is not atypical (Jimenez et al., 2009).
444

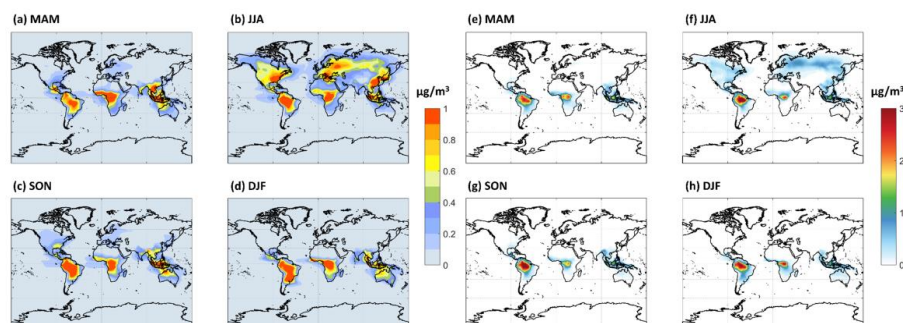
445 For comparison, we also show seasonal PBL distributions of HOM-RO₂ self or cross reaction
446 accretion products, assuming the C₂₀-HOM are formed at unit yield. This assumption
447 provides an upper-limit, but one which is supported by some laboratory studies. Throughout
448 the tropical forests and boreal regions during summer, HOM-RO₂ accretion products in this
449 simulation reach 3 or $1 \mu\text{g m}^{-3}$, respectively. As total OA in some boreal and tropical forest
450 measurements can be on this order (Jimenez et al., 2009; Lee et al., 2018; de Sa et al., 2018)
451 outside of biomass burning periods, we conclude C₂₀-HOM undergo particle phase
452 decomposition and/or the HOM-RO₂ self and cross reactions do not produce accretion
453 products at unit yield or the model underestimates NO throughout boreal and tropical forest
454 regions which would suppress both HOM and more so HOM accretion product
455 concentrations. As shown in the SI (Figure S7), assuming an accretion product branching of 4%
456 for all MT-RO₂ self or cross reactions, including HOM-RO₂, leads to significantly lower, but not
457 unimportant, concentrations of accretion products. The total C₁₅ + C₂₀ accretion product
458 concentrations in the PBL of tropical and boreal forest regions are typically less than 1 or
459 $0.25 \mu\text{g m}^{-3}$, respectively, in this simulation.
460

461 Accretion products from HOM-RO₂ reactions with other HOM-RO₂ are likely an important
462 route to new particle formation especially in the relatively warm planetary boundary layer.
463 Thus, to predict new particle formation in regions such as the remote temperate or boreal
464 forests, such accretion products will need to be incorporated. As noted above, the self and
465 cross reaction rates and accretion product branching in both cases are far larger than those
466 commonly used in GEOS-Chem. Nucleation and growth of particles by MT-HOM and
467 associated accretion products is beyond the scope here, but in both treatments of accretion
468 product formation, C₂₀ HOM accretion products reach concentrations which are likely
469 relevant for participation in new particle formation (e.g. 10^7 - $10^8 \text{ molec cm}^{-3}$) to the extent it
470 occurs in the PBL over forested regions (Bianchi et al., 2019). A remaining question is to what
471 extent MT-RO₂ derived accretion products more generally form and contribute to OA mass.
472

473 Our results suggest that further refinement of HOM formation and loss kinetics is needed
474 since the range of our simulations suggest HOM either make relatively small contributions to
475 regional OA or constitute the majority of OA outside of biomass burning periods over



476 tropical forests year-round, and during summer months for temperate and boreal forests.
477 Figure 8 illustrates that for two of the sensitivity simulations which bound possible HOM
478 formation and loss kinetics, MT-HOM concentrations alone are either 5 to 10% of total OA
479 predicted by the standard GEOS-Chem model or are more than a factor of 1.5 higher than
480 the predicted total OA. Incorporating predicted MT-RO₂ derived C₁₅ and C₂₀ accretion
481 products as an OA source only increases the potential contribution of MT to total OA. If the
482 MT-RO₂ accretion product branching is on average 4%, accretion products can double the
483 contribution of MT to OA when HOM are simulated in the LowProd_Photo case (see Figure
484 S7). If the accretion branching ratio is closer to unity, as expected for HOM-RO₂, the
485 contribution of HOM monomers and MT-HOM accretion products to OA is even larger,
486 reaching or exceeding a mean ratio of 3 in tropical forests compared to GEOS-Chem
487 predicted OA. Thus, revising MT chemistry to incorporate gas-phase sources of low and
488 extremely low volatility pathways will likely increase, perhaps substantially, the total OA
489 predicted by the GEOS-Chem model over forested regions.

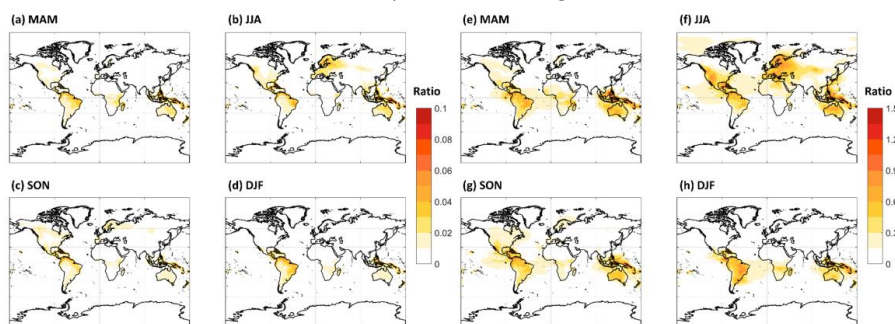


491
492 **Figure 7.** The seasonal PBL-averaged total HOM mass concentrations of (a) MAM, (b) JJA (c)
493 SON and (d) DJF from experiment LowProd_noPhoto. Seasonal PBL-averaged total C₂₀ HOM
494 accretion products are shown in panels e-h, assuming HOM-RO₂ self and cross reactions
495 produce accretion products at unit yield.

496
497 There are limited observations of HOM that can be used to investigate the validity of the
498 different scenarios simulated here. First, the majority of HOM will condense to form SOA,
499 where they may further react to form products that might not be traceable to HOM formed
500 in the gas-phase (Krapf et al., 2016; Lee et al., 2020; Pospisilova et al., 2020; Zawadowicz et
501 al., 2020). Second, most HOM have been observed only in the gas-phase (Bianchi et al., 2016;
502 Ehn et al., 2014; Massoli et al., 2018), which represents only a local steady-state between the
503 formation and condensation sink over small spatial scales compared to the current model
504 resolution. The FIGAERO HRToF-CIMS instrument measures some HOM in both the gas and
505 particle phases, while the aerosol mass spectrometer (AMS) provides an upper limit
506 constraint on the total organic aerosol. In Figure 8, we show observations from the FIGAERO
507 HRToF-CIMS at a rural temperate and rural boreal forest, in Centreville, AL in the Southeast
508 U.S. and SMEAR II station in Hyytiälä, Finland, respectively. In addition, we show AMS
509 observations of total OA from these sites as well as from the T3 site of the Go-Amazon



510 campaign outside of Manaus, Brazil. The Centreville, AL observations were obtained in
511 June–July 2013, the SMEAR II observations were from April–June 2014, and the Go-Amazon
512 observations were from February–March 2014. More information can be found in SI and
513 related papers (Carlton et al., 2018; Martin et al., 2016; Petaja et al., 2016). The FIGAERO
514 HRToF-CIMS observations include both speciated HOM organic nitrates and non-nitrates.



515
516 **Figure 8.** The seasonal PBL-averaged total C_{10} -HOM mass concentrations from the
517 LowProd_Photo (a-d) or the HighProd_noPhoto (e-h) simulations plotted relative to the total
518 OA mass concentration predicted by GEOS-Chem for the same periods and locations. Note
519 the color scale for panels a-d (0 to 0.1) is about a factor of 10 lower than that for panels e-h
520 (0 to 1.5).

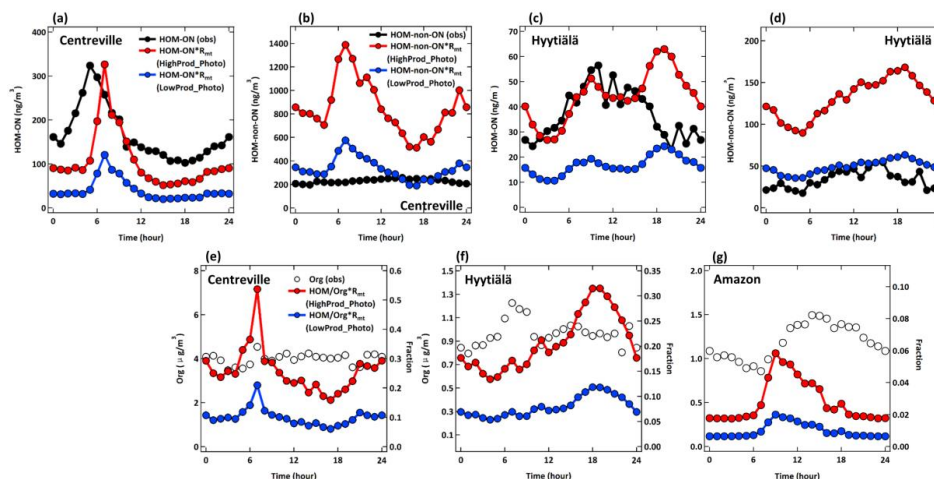
521
522 We compare these observations to two simulations, HighProd_Photo and LowProd_Photo,
523 where each includes photochemical losses of HOM based on recent experimental work
524 (Zawadowicz et al., 2020), but different yields of MT- bRO_2 that can undergo unimolecular
525 H-shifts as discussed above. The comparison is challenged for a number of reasons. First,
526 monoterpene emissions are uncertain in a global sense but will also vary significantly at
527 scales below the resolution of the model. Second, gas-phase HOM will be sensitive to the
528 local oxidant conditions, while particulate HOM potentially represent the integral of multiple
529 days of formation, loss, and transport. Moreover, HOM in the particle phase may react into
530 non-HOM, be lost on instrument surfaces, or thermally decompose during the analysis, such
531 that observations of total HOM are possibly underestimated by the FIGAERO HRToF-CIMS
532 instrument. To facilitate the comparison, we use the diurnal cycle in observations averaged
533 over 4 to 6 weeks of observations to minimize the impact of meteorological variability. We
534 scale the predicted HOM concentrations in the lowest model level by the ratio of observed to
535 predicted monoterpene concentrations in order to account for potential biases in the
536 monoterpene emissions (Figure S8). For SOAS and GoAmazon, we use the hourly average
537 measured monoterpene data to compare with the hourly GEOS-Chem predictions, while for
538 the BAEC campaign at SMEAR II station, we use the campaign average of measured
539 monoterpene concentrations. We separate HOM organic nitrates (ON) from HOM
540 non-nitrates (non-ON) where possible but compare to the total measured gas + particle in
541 each category.

542
543 As shown in Figure 9, there is general order-of-magnitude agreement between the observed
544 HOM and those predicted by one of the model simulations when adjusted by the predicted



545 and observed monoterpene concentrations as described above. The HighProd_Photo
546 simulation is better able to simulate the HOM-ON, but overestimates the non-ON HOM
547 measured in the boreal forest location. In contrast, in the Centreville location, the
548 HighProd_Photo simulation underestimates the measured HOM-ON but overestimates the
549 measured non-ON HOM. The general overestimation of observed non-ON HOM could be due
550 to the non-ON HOM having reacted in the particle phase into components that are not
551 detectable as HOM due to analytical limitations of the instrument used, which relies on
552 thermal desorption and thus can be subject to thermal decomposition of low volatility
553 components [Lopez-Hilfiker et al., 2014]. We note that the HighProd_Photo simulation does
554 not overestimate the observed fine mode OA mass concentrations in any of the three
555 locations, such that there is potential for a higher fraction of MT oxidation to result in HOM
556 and higher contributions of MT-HOM to OA than shown in Figure 9. The reason for a low
557 contribution of MT-HOM to OA predicted for the Amazon region remains unknown, but
558 possibly related to errors in the modeled MT emission inventory, limitations of comparing a
559 relatively coarse model resolution to a single location measurement, and/or the influences
560 from isoprene, biomass burning, and other pathways are perhaps more important in this
561 location.

562
563 The general shape of the HOM diurnal cycle and HOM relative to OA (Figure 9) are typically
564 well captured for each location, except for the late evening and early morning periods
565 possibly due to issues simulating the nocturnal layer relative to the emission height of
566 monoterpenes. In the Amazon location, there is a clear late afternoon peak in the measured
567 OA that is not present in the predicted monoterpene derived HOM concentrations. These
568 comparisons suggest that based on the current set of observations we cannot conclude
569 which set of HOM formation and loss kinetics is most appropriate for describing ambient
570 HOM. We can conclude that total HOM abundances, including both ON and non-ON HOM,
571 are potentially higher than those shown in Figure 9, similar to those predicted by the
572 HighProd_Photo case or the LowProd_noPhoto case, with PBL average mass concentrations
573 in monoterpene rich regions and seasons of order 0.5 to 1 $\mu\text{g m}^{-3}$, see, e.g., Figures S9 and
574 S10. Uncertainties in first-generation RO_2 branching parameters, isomerization rate constants,
575 and HOM chemical fate remain large, with limited observational constraints on total HOM
576 concentrations (gas + particle).
577



578

579 **Figure 9.** Diurnal changes of observed (black line) and simulated (HighProd_Photo: red line;
580 LowProd_Photo: blue line) (a) HOM-ON and (b) HOM-non-ON mass concentrations at
581 Centreville site. (c)-(d) The same as (a)-(b) but at Hyttiälä site. (e)-(f) Diurnal changes of
582 observed organic aerosol mass concentrations (black hollow circle markers) and the fractions
583 that simulated total HOM account for of observed organic aerosols (HighProd_Photo: red;
584 LowProd_Photo: blue) at Centreville, Hyttiälä and Amazon sites, respectively.

585

586 3.4 Vertical profiles of HOM

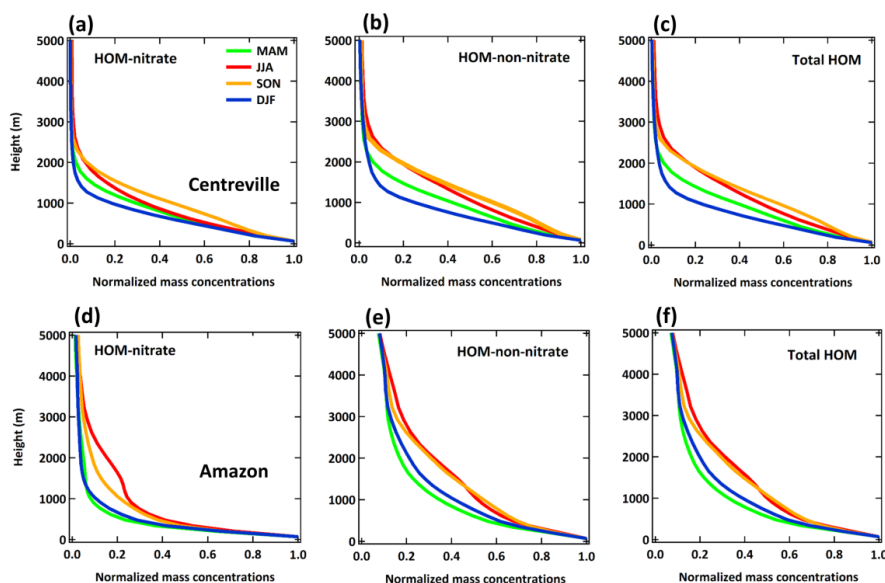
587 Figure 10 summarizes the vertical distribution of HOM predicted by the LowProd_Photo
588 simulation for two locations, one over the SE US SOAS site and one over the Amazon region
589 using the same grid which contains the GoAmazon T3 site (Martin et al., 2016). Evident is the
590 expected predominance of monoterpene present within the PBL in all seasons and locations
591 related to the surface vegetation source. Also evident is the different vertical profiles of
592 HOM-ON compared to non-ON HOM, with slower decays with altitude of non-ON HOM up to
593 2 to 3 km above the surface during JJA in both the SEUS and Amazon regions, likely due to
594 changes in the HOM-RO₂ fate with altitude (see 3.1). Over the Amazon during JJA and SON,
595 both non-ON HOM and HOM-ON concentrations are predicted to be relatively enhanced
596 between 1 to 5 km compared to the lowest altitude concentrations. The relative
597 enhancement in this altitude region during JJA and SON compared to DJF and MAM likely
598 reflects overall drier conditions but also significant vertical transport of HOM precursors
599 during these seasons, e.g. through shallow convection. The relative enhancements
600 specifically between 1 to 4 km compared to altitudes higher than 5 km could also reflect the
601 temperature dependence of the unimolecular H-shift rate constant describing monoterpene
602 derived RO₂ autoxidation and changing biomolecular reaction rates with altitude. This
603 relative enhancement is not as obvious in the vertical profiles over the SEUS, which appear
604 as smoother monotonic decays with altitude, and that are higher in abundance during
605 summer months.

606

607 HOM-RO₂ accretion products illustrate similar vertical profiles as the HOM monomers (see SI



608 Figures S12 and S13). If we use the rate constants reported by Berndt et al., (2018a, 2018b)
609 together with branching ratio of unity for HOM-RO₂ derived accretion products, the seasonal
610 mean abundance of predicted total of C₁₅ and C₂₀ HOM accretion products reaches 1 to 5 μg
611 m⁻³ in the PBL over the SE US and tropical forested regions respectively (see SI), and decay to
612 1×10⁻³ and 3×10⁻² μg m⁻³ (1×10⁶ and 4×10⁷ molec cm⁻³), respectively, in the upper troposphere
613 over these regions. Assuming instead a HOM-RO₂ accretion product yield of 4%, the
614 predicted total of C₁₅ and C₂₀ HOM accretion products are between 0.2 and 1 μg m⁻³ over the
615 SE US and tropical forests, respectively, decaying to 2×10⁻⁴ and 7×10⁻³ μg m⁻³ (3×10⁵ and 1×10⁷
616 molec cm⁻³) in the upper troposphere. At such *average* concentrations in the upper
617 troposphere over these regions, we conclude either type of HOM accretion product will
618 likely contribute significantly to new particle formation and growth, but uncertainty in the
619 accretion product branching of HOM-RO₂ reactions would lead to a factor of 4 or more in the
620 estimated contribution.
621



622
623 **Figure 10.** The seasonal averaged vertical profiles of HOM-ON (left panel), HOM-non-ON
624 (middle panel) and total HOM (right panel) at Centreville (top panel) and Amazon (bottom
625 panel). All the results are from experiment LowProd_Photo. Values are normalized to the
626 lowest-level values of each season. The profiles with absolute concentrations are shown in
627 Figure S9.

628
629 **4. Conclusion**

630 We implemented a new mechanism to describe MT-derived RO₂ chemistry in the
631 GEOS-Chem global chemical transport model. The mechanism is relatively simple, adding 10
632 species and 37 reactions to the standard mechanism, without substantial addition of
633 computation time. We focused on updating the representation of unimolecular H-shift
634 reactions to form HOM-RO₂ and their fate, as well as the self- and cross-reactions of



635 MT-derived RO₂ and isoprene derived RO₂. Several sensitivity studies were conducted to
636 evaluate the impact of various mechanism parameters and associated uncertainties, and
637 where possible we compared to observations. The results from these sensitivity studies show
638 that for a model resolution of 2° × 2.5°, uncertainty in the average H-shift rate constant is less
639 important for predicted HOM concentrations than the fraction of MT reactions with OH or O₃
640 to form RO₂ which can undergo H-shift and autoxidation and the photochemical lifetime of
641 HOM. While a comprehensive comparison of HOM predictions to OA remains, in three
642 locations, the model predictions of HOM did not exceed total measured OA mass
643 concentrations, which is currently the strongest constraint on HOM. However, using
644 HOM-ON measurements as a guide suggests that if the fraction of MT-RO₂ that undergo
645 relatively rapid H-shift ($k_{\text{auto}} > 0.1 \text{ s}^{-1}$) is greater than 0.25, then significant photochemical
646 losses of HOM mass from particles that is faster than wet or dry deposition of particulate
647 organics is required. Additional refinement of the branching to MT-RO₂ which can undergo
648 H-shifts and mechanistic insights into HOM photochemical lifetime are clearly needed. That
649 current estimates of MT-derived HOM monomer and HOM accretion product formation
650 rates from laboratory studies lead to mass concentrations of the same order as OA mass
651 concentrations predicted by the model, a comprehensive online coupling of this updated
652 MT-RO₂ chemistry to aerosol formation in GEOS-Chem and other models is needed.

653
654 The majority of HOM production occurs in the continental boundary layer where MT
655 emissions are significant, including boreal, temperate and tropical regions. H-shift and
656 autoxidation is the major fate for the subset of MT-RO₂ with that capability, outcompeting
657 reactions with NO, HO₂ and RO₂ up to 6 km altitude in relatively unpolluted regions.
658 Autoxidation of first-generation MT-RO₂ is significantly slower in the upper troposphere and
659 likely uncompetitive with reactions with NO and HO₂. As such, HOM formation in the outflow
660 of deep convection is unlikely, though HOM formation from MT detraining from shallow
661 convection below 6 km is feasible.

662
663 Implementing faster self and cross-reactions between RO₂ as found by Berndt et al. (2018a)
664 lead to significantly lower HO₂ and RO₂ concentrations in boreal and tropical forested regions (by
665 20% or more compared to the standard mechanism), but globally average changes in OH, NO_x,
666 and O₃ are negligible. These reactions also alter the fate of MT-RO₂, especially MT-derived
667 HOM-RO₂, for which reaction with RO₂ is the dominant fate throughout the boundary layer
668 neglecting unimolecular HOM-RO₂ reactions. Such a situation can be supported by the molecular
669 composition measurements of MT-HOM which show significant contributions of HOM with H
670 numbers less than 16 and odd-numbers of O, e.g., C₁₀H₁₄O₉. This evidence alone is not sufficient,
671 as HOM-RO₂ reactions with NO could also produce similar results. Moreover, the branching to
672 accretion products is a key parameter with significantly different ranges produced by laboratory
673 studies. The concentrations of C₁₅ and C₂₀ accretion products predicted using self and
674 cross-reaction rate constants of $\sim 10^{-11}$ - $10^{-10} \text{ cm}^3 \text{ molec}^{-1} \text{ s}^{-1}$ with a conservative branching (4%)
675 from Zhao et al (2018), are typically small compared to average OA mass concentrations, except
676 in the tropical forested regions, where these accretion products alone are likely similar to
677 background OA concentrations outside of biomass burning events. Using a larger branching to
678 accretion products as supported by studies by Berndt et al (2018) leads to such accretion



679 products likely dominating low volatility products that could contribute to OA, with predicted
680 mass concentrations well exceeding OA mass concentrations in remote tropical regions. Thus,
681 further refinement in the rate constants and branching to gas-phase accretion products and their
682 photochemical fates are needed, especially since these products from HOM-RO₂ cross reactions
683 are likely essential in the contributions of MT to new particle formation (Bianchi et al., 2019;
684 McFiggans et al., 2019) especially over tropical forested regions (Andreae et al., 2018; Wang et al.,
685 2016; Zhao et al., 2020).

686

687 **Acknowledgements**

688 JAT was supported by a grant from the National Science Foundation (CHE-1807204) and the U.S.
689 Department of Energy Atmospheric Science Research program (DE-SC0021097). RX thanks
690 Nanjing University for an undergraduate research fellowship.

691

692 **References Cited**

693 Amos, H. M., Jacob, D. J., Holmes, C. D., Fisher, J. A., Wang, Q., Yantosca, R. M., Corbitt, E. S.,
694 Galarneau, E., Rutter, A. P., Gustin, M. S., Steffen, A., Schauer, J. J., Graydon, J. A., St Louis, V.
695 L., Talbot, R. W., Edgerton, E. S., Zhang, Y. and Sunderland, E. M.: Gas-particle partitioning of
696 atmospheric Hg(II) and its effect on global mercury deposition, *Atmos. Chem. Phys.*, 12(1),
697 591–603, doi:10.5194/acp-12-591-2012, 2012.

698 Andreae, M. O., Afchine, A., Albrecht, R., Holanda, B. A., Artaxo, P., Barbosa, H. M. J., Borrmann,
699 S., Cecchini, M. A., Costa, A., Dollner, M., Fuetterer, D., Jaervinen, E., Jurkat, T., Klimach, T.,
700 Konemann, T., Knote, C., Kraemer, M., Krisna, T., Machado, L. A. T., Mertes, S., Minikin, A.,
701 Poehlker, C., Poehlker, M. L., Poeschl, U., Rosenfeld, D., Sauer, D., Schlager, H., Schnaiter, M.,
702 Schneider, J., Schulz, C., Spanu, A., Sperling, V. B., Voigt, C., Walser, A., Wang, J., Weinzierl, B.,
703 Wendisch, M. and Ziereis, H.: Aerosol characteristics and particle production in the upper
704 troposphere over the Amazon Basin, *Atmos. Chem. Phys.*, 18(2), 921–961,
705 doi:10.5194/acp-18-921-2018, 2018.

706 Arneth, A., Monson, R. K., Schurgers, G., Niinemets, Ü. and Palmer, P. I.: Why are estimates of
707 global terrestrial isoprene emissions so similar (and why is this not so for monoterpenes)?,
708 *Atmos. Chem. Phys.*, 8(16), 4605–4620, doi:10.5194/acp-8-4605-2008, 2008.

709 Berndt, T., Richters, S., Jokinen, T., Hyttinen, N., Kurtén, T., Otkjær, R. V., Kjaergaard, H. G.,
710 Stratmann, F., Herrmann, H., Sipilä, M., Kulmala, M. and Ehn, M.: Hydroxyl radical-induced
711 formation of highly oxidized organic compounds, *Nat. Commun.*, 7(May), 13677,
712 doi:10.1038/ncomms13677, 2016.

713 Berndt, T., Mentler, B., Scholz, W., Fischer, L., Herrmann, H., Kulmala, M. and Hansel, A.:
714 Accretion Product Formation from Ozonolysis and OH Radical Reaction of α -Pinene:
715 Mechanistic Insight and the Influence of Isoprene and Ethylene, *Environ. Sci. Technol.*,
716 doi:10.1021/acs.est.8b02210, 2018a.

717 Berndt, T., Scholz, W., Mentler, B., Fischer, L., Herrmann, H., Kulmala, M. and Hansel, A.:
718 Accretion Product Formation from Self- and Cross-Reactions of RO₂ Radicals in the
719 Atmosphere, *Angew. Chemie Int. Ed.*, 57(14), 3820–3824,
720 doi:https://doi.org/10.1002/anie.201710989, 2018b.

721 Bey, I., Jacob, D. J., Yantosca, R. M., Logan, J. A., Field, B. D., Fiore, A. M., Li, Q.-B., Liu, H.-Y.,
722 Mickley, L. J. and Schultz, M. G.: Global Modeling of Tropospheric Chemistry with Assimilated



- 723 Meteorology: Model Description and Evaluation, *J. Geophys. Res.*, **106**, 73–95,
724 doi:10.1029/2001JD000807, 2001.
- 725 Bianchi, F., Trostl, J., Junninen, H., Frege, C., Henne, S., Hoyle, C. R., Molteni, U., Herrmann, E.,
726 Adamov, A., Bukowiecki, N., Chen, X., Duplissy, J., Gysel, M., Hutterli, M., Kangasluoma, J.,
727 Kontkanen, J., Kuerten, A., Manninen, H. E., Muench, S., Perakyla, O., Petaja, T., Rondo, L.,
728 Williamson, C., Weingartner, E., Curtius, J., Worsnop, D. R., Kulmala, M., Dommen, J. and
729 Baltensperger, U.: New particle formation in the free troposphere: A question of chemistry
730 and timing, *Science* (80-.), **352**(6289), 1109–1112, doi:10.1126/science.aad5456, 2016.
- 731 Bianchi, F., Kurten, T., Riva, M., Mohr, C., Rissanen, M. P., Roldin, P., Berndt, T., Crouse, J. D.,
732 Wennberg, P. O., Mentel, T. F., Wildt, J., Junninen, H., Jokinen, T., Kulmala, M., Worsnop, D. R.,
733 Thornton, J. A., Donahue, N., Kjaergaard, H. G. and Ehn, M.: Highly Oxygenated Organic
734 Molecules (HOM) from Gas-Phase Autoxidation Involving Peroxy Radicals: A Key Contributor
735 to Atmospheric Aerosol, *Chem. Rev.*, **119**(6), 3472–3509, doi:10.1021/acs.chemrev.8b00395,
736 2019.
- 737 Carlton, A. G., de Gouw, J., Jimenez, J. L., Ambrose, J. L., Attwood, A. R., Brown, S., Baker, K. R.,
738 Brock, C., Cohen, R. C., Edgerton, S., Farkas, C. M., Farmer, D., Goldstein, A. H., Gratz, L.,
739 Guenther, A., Hunt, S., Jaeglé, L., Jaffe, D. A., Mak, J., McClure, C., Nenes, A., Nguyen, T. K.,
740 Pierce, J. R., de Sa, S., Selin, N. E., Shah, V., Shaw, S., Shepson, P. B., Song, S., Stutz, J., Surratt,
741 J. D., Turpin, B. J., Warneke, C., Washenfelder, R. A., Wennberg, P. O. and Zhou, X.: Synthesis
742 of the Southeast Atmosphere Studies: Investigating Fundamental Atmospheric Chemistry
743 Questions, *Bull. Am. Meteorol. Soc.*, **99**(3), 547–567, doi:10.1175/BAMS-D-16-0048.1, 2018.
- 744 DeCarlo, P. F., Kimmel, J. R., Trimborn, A., Northway, M. J., Jayne, J. T., Aiken, A. C., Gonin, M.,
745 Fuhrer, K., Horvath, T., Docherty, K. S., Worsnop, D. R. and Jimenez, J. L.: Field-Deployable,
746 High-Resolution, Time-of-Flight Aerosol Mass Spectrometer, *Anal. Chem.*, **78**(24), 8281–8289,
747 doi:10.1021/ac061249n, 2006.
- 748 Ehn, M., Thornton, J. A., Kleist, E., Sipila, M., Junninen, H., Pullinen, I., Springer, M., Rubach, F.,
749 Tillmann, R., Lee, B., Lopez-Hilfiker, F., Andres, S., Acir, I.-H., Rissanen, M., Jokinen, T.,
750 Schobesberger, S., Kangasluoma, J., Kontkanen, J., Nieminen, T., Kurten, T., Nielsen, L. B.,
751 Jorgensen, S., Kjaergaard, H. G., Canagaratna, M., Dal Maso, M., Berndt, T., Petaja, T., Wahner,
752 A., Kerminen, V.-M., Kulmala, M., Worsnop, D. R., Wildt, J. J., Mentel, T. F., Maso, M. D.,
753 Berndt, T., Petaja, T., Wahner, A., Kerminen, V.-M., Kulmala, M., Worsnop, D. R., Wildt, J. J.
754 and Mentel, T. F.: A large source of low-volatility secondary organic aerosol, *Nature*,
755 **506**(7489), 476–479, doi:10.1038/nature13032, 2014.
- 756 Fisher, J. A., Jacob, D. J., Travis, K. R., Kim, P. S., Marais, E. A., Chan Miller, C., Yu, K., Zhu, L.,
757 Yantosca, R. M., Sulprizio, M. P., Mao, J., Wennberg, P. O., Crouse, J. D., Teng, A. P., Nguyen,
758 T. B., St. Clair, J. M., Cohen, R. C., Romer, P., Nault, B. A., Wooldridge, P. J., Jimenez, J. L.,
759 Campuzano-Jost, P., Day, D. A., Hu, W., Shepson, P. B., Xiong, F., Blake, D. R., Goldstein, A. H.,
760 Misztal, P. K., Hanisco, T. F., Wolfe, G. M., Ryerson, T. B., Wisthaler, A. and Mikoviny, T.:
761 Organic nitrate chemistry and its implications for nitrogen budgets in an isoprene- and
762 monoterpene-rich atmosphere: constraints from aircraft (SEAC⁴RS) and ground-based
763 (SOAS) observations in the Southeast US, *Atmos. Chem. Phys.*, **16**(9), 5969–5991,
764 doi:10.5194/acp-16-5969-2016, 2016.
- 765 Gelaro, R., McCarty, W., Suárez, M. J., Todling, R., Molod, A., Takacs, L., Randles, C. A., Darmenov,
766 A., Bosilovich, M. G., Reichle, R. and others: The modern-era retrospective analysis for



- 767 research and applications, version 2 (MERRA-2), *J. Clim.*, 30(14), 5419–5454, 2017.
- 768Guenther, A. B., Jiang, X., Heald, C. L., Sakulyanontvittaya, T., Duhl, T., Emmons, L. K. and Wang, X.:
769 The model of emissions of gases and aerosols from nature version 2.1 (MEGAN2.1): An
770 extended and updated framework for modeling biogenic emissions, *Geosci. Model Dev.*, 5(6),
771 1471–1492, doi:10.5194/gmd-5-1471-2012, 2012.
- 772Hallquist, M., Wenger, J. C., Baltensperger, U., Rudich, Y., Simpson, D., Claeys, M., Dommen, J.,
773 Donahue, N. M., George, C., Goldstein, A. H., Hamilton, J. F., Herrmann, H., Hoffmann, T.,
774 Iinuma, Y., Jang, M., Jenkin, M. E., Jimenez, J. L., Kiendler-Scharr, A., Maenhaut, W.,
775 McFiggans, G., Mentel, T. F., Monod, A., Prévôt, A. S. H., Seinfeld, J. H., Surratt, J. D.,
776 Szmigielski, R. and Wildt, J.: The formation, properties and impact of secondary organic
777 aerosol: current and emerging issues, *Atmos. Chem. Phys.*, 9(14), 5155–5236,
778 doi:10.5194/acp-9-5155-2009, 2009.
- 779Iyer, S., Rissanen, M. P., Valiev, R., Barua, S., Krechmer, J. E., Thornton, J., Ehn, M. and Kurtén, T.:
780 Molecular mechanism for rapid autoxidation in α -pinene ozonolysis, *Nat. Commun.*, 12(1),
781 878, doi:10.1038/s41467-021-21172-w, 2021.
- 782Jayne, J. T., Leard, D. C., Zhang, X., Davidovits, P., Smith, K. A., Kolb, C. E. and Worsnop, D. R.:
783 Development of an Aerosol Mass Spectrometer for Size and Composition Analysis of
784 Submicron Particles, *Aerosol Sci. Technol.*, 33(1–2), 49–70, doi:10.1080/027868200410840,
785 2000.
- 786Jimenez, J. L., Canagaratna, M. R., Donahue, N. M., Prevot, A. S. H., Zhang, Q., Kroll, J. H., DeCarlo,
787 P. F., Allan, J. D., Coe, H., Ng, N. L., Aiken, A. C., Docherty, K. S., Ulbrich, I. M., Grieshop, A. P.,
788 Robinson, A. L., Duplissy, J., Smith, J. D., Wilson, K. R., Lanz, V. A., Hueglin, C., Sun, Y. L., Tian,
789 J., Laaksonen, A., Raatikainen, T., Rautiainen, J., Vaattovaara, P., Ehn, M., Kulmala, M.,
790 Tomlinson, J. M., Collins, D. R., Cubison, M. J., Dunlea, J., Huffman, J. A., Onasch, T. B., Alfarra,
791 M. R., Williams, P. I., Bower, K., Kondo, Y., Schneider, J., Drewnick, F., Borrmann, S., Weimer, S.,
792 Demerjian, K., Salcedo, D., Cottrell, L., Griffin, R., Takami, A., Miyoshi, T., Hatakeyama, S.,
793 Shimono, A., Sun, J. Y., Zhang, Y. M., Dzepina, K., Kimmel, J. R., Sueper, D., Jayne, J. T.,
794 Herndon, S. C., Trimborn, A. M., Williams, L. R., Wood, E. C., Middlebrook, A. M., Kolb, C. E.,
795 Baltensperger, U. and Worsnop, D. R.: Evolution of Organic Aerosols in the Atmosphere,
796 *Science (80-.)*, 326(5959), 1525–1529, doi:10.1126/science.1180353, 2009.
- 797Jokinen, T., Berndt, T., Makkonen, R., Kerminen, V.-M., Junninen, H., Paasonen, P., Stratmann, F.,
798 Herrmann, H., Guenther, A. B., Worsnop, D. R., Kulmala, M., Ehn, M. and Sipilä, M.:
799 Production of extremely low volatile organic compounds from biogenic emissions: Measured
800 yields and atmospheric implications., *Proc. Natl. Acad. Sci. U. S. A.*, 112(23), 7123–8,
801 doi:10.1073/pnas.1423977112, 2015.
- 802Keller, C. A., Long, M. S., Yantosca, R. M., Da Silva, A. M., Pawson, S. and Jacob, D. J.: HEMCO v1.0:
803 a versatile, ESMF-compliant component for calculating emissions in atmospheric models,
804 *Geosci. Model Dev.*, 7(4), 1409–1417, doi:10.5194/gmd-7-1409-2014, 2014.
- 805Krapf, M., El Haddad, I., Bruns, E. A., Molteni, U., Daellenbach, K. R., Prévôt, A. S. H.,
806 Baltensperger, U., Dommen, J., Berndt, T., Richters, S., Kaethner, R., Voigtländer, J., Stratmann,
807 F., Sipilä, M., Kulmala, M., Herrmann, H., Crouse, J. D., Nielsen, L. B., Jørgensen, S.,
808 Kjaergaard, H. G., Wennberg, P. O., Ehn, M., Thornton, J. A., Kleist, E., Sipilä, M., Junninen, H.,
809 Pullinen, I., Springer, M., Rubach, F., Tillmann, R., Lee, B., et Al., Jokinen, T., Berndt, T.,
810 Makkonen, R., Kerminen, V.-M., Junninen, H., Paasonen, P., Stratmann, F., Herrmann, H.,



- 811 Guenther, A. B., Worsnop, D. R., et Al., Jokinen, T., Sipilä, M., Richters, S., Kerminen, V.-M.,
812 Paasonen, P., Stratmann, F., Worsnop, D., Kulmala, M., Ehn, M., Herrmann, H., Berndt, T.,
813 Mentel, T. F., Springer, M., Ehn, M., Kleist, E., Pullinen, I., Kurtén, T., Rissanen, M., Wahner, A.,
814 Wildt, J., Richters, S., Herrmann, H., Berndt, T., Rissanen, M. P., Kurtén, T., Sipilä, M.,
815 Thornton, J. A., Kangasluoma, J., Sarnela, N., Junninen, H., Jørgensen, S., Schallhart, S., Kajos,
816 M. K., et Al., Heaton, K. J., Dreyfus, M. A., Wang, S., Johnston, M. V, Reinnig, M.-C., Warnke, J.,
817 Hoffmann, T., Ziemann, P. J., Aimanant, S., Ziemann, P. J., Docherty, K. S., Wu, W., Lim, Y. B.,
818 Ziemann, P. J., Mertes, P., Pfaffenberger, L., Dommen, J., Kalberer, M., Baltensperger, U.,
819 Nguyen, T. B., Bateman, A. P., Bones, D. L., et al.: Labile Peroxides in Secondary Organic
820 Aerosol, *Chem*, 1(4), 603–616, doi:10.1016/j.chempr.2016.09.007, 2016.
- 821Kulmala, M., Petäjä, T., Ehn, M., Thornton, J., Sipilä, M., Worsnop, D. R. and Kerminen, V.-M.:
822 Chemistry of Atmospheric Nucleation: On the Recent Advances on Precursor
823 Characterization and Atmospheric Cluster Composition in Connection with Atmospheric New
824 Particle Formation, *Annu. Rev. Phys. Chem.*, 65(1),
825 doi:doi:10.1146/annurev-physchem-040412-110014, 2014.
- 826Kurten, T., Rissanen, M. P., Mackeprang, K., Thornton, J. A., Hyttinen, N., Jorgensen, S., Ehn, M.,
827 Kjaergaard, H. G., Kurtén, T., Rissanen, M. P., Mackeprang, K., Thornton, J. A., Hyttinen, N.,
828 Jørgensen, S., Ehn, M. and Kjaergaard, H. G.: Computational Study of Hydrogen Shifts and
829 Ring-Opening Mechanisms in α -Pinene Ozonolysis Products, *J. Phys. Chem. A*, 119(46),
830 11366–11375, doi:10.1021/acs.jpca.5b08948, 2015.
- 831Lee, B. H., Mohr, C., Lopez-Hilfiker, F. D., Lutz, A., Hallquist, M., Lee, L., Romer, P., Cohen, R. C.,
832 Iyer, S., Kurten, T., Hu, W., Day, D. A., Campuzano-Jost, P., Jimenez, J. L., Xu, L., Ng, N. L., Guo,
833 H., Weber, R. J., Wild, R. J., Brown, S. S., Koss, A., de Gouw, J., Olson, K., Goldstein, A. H., Seco,
834 R., Kim, S., McAvey, K., Shepson, P. B., Starn, T., Baumann, K., Edgerton, E. S., Liu, J., Shilling, J.
835 E., Miller, D. O., Brune, W., Schobesberger, S., D'Ambro, E. L., Thornton, J. A., Kurtén, T., Hu,
836 W., Day, D. A., Campuzano-Jost, P., Jimenez, J. L., Xu, L., Ng, N. L., Guo, H., Weber, R. J., Wild,
837 R. J., Brown, S. S., Koss, A., de Gouw, J., Olson, K., Goldstein, A. H., Seco, R., Kim, S., McAvey,
838 K., Shepson, P. B., Starn, T., Baumann, K., Edgerton, E. S., Liu, J., Shilling, J. E., Miller, D. O.,
839 Brune, W., Schobesberger, S., D\textquoterightAmbro, E. L. and Thornton, J. A.: Highly
840 functionalized organic nitrates in the southeast United States: Contribution to secondary
841 organic aerosol and reactive nitrogen budgets, *Proc. Natl. Acad. Sci.*, 113(6), 1516–1521,
842 doi:10.1073/pnas.1508108113, 2016.
- 843Lee, B. H., Lopez-Hilfiker, F. D., D'Ambro, E. L., Zhou, P., Boy, M., Petaja, T., Hao, L., Virtanen, A.
844 and Thornton, J. A.: Semi-volatile and highly oxygenated gaseous and particulate organic
845 compounds observed above a boreal forest canopy, *Atmos. Chem. Phys.*, 18(15), 11547–
846 11562, doi:10.5194/acp-18-11547-2018, 2018.
- 847Lee, B. H., D'Ambro, E. L., Lopez-Hilfiker, F. D., Schobesberger, S., Mohr, C., Zawadowicz, M. A., Liu,
848 J., Shilling, J. E., Hu, W., Palm, B. B., Jimenez, J. L., Hao, L., Virtanen, A., Zhang, H., Goldstein,
849 A. H., Pye, H. O. T. and Thornton, J. A.: Resolving Ambient Organic Aerosol Formation and
850 Aging Pathways with Simultaneous Molecular Composition and Volatility Observations, *ACS*
851 *Earth Sp. Chem.*, 4(3), 391–402, doi:10.1021/acsearthspacechem.9b00302, 2020.
- 852Liu, H., Jacob, D. J., Bey, I. and Yantosca, R. M.: Constraints from ^{210}Pb and ^7Be on wet
853 deposition and transport in a global three-dimensional chemical tracer model driven by
854 assimilated meteorological fields, *J. Geophys. Res. Atmos.*, 106(D11), 12109–12128,



- 855 doi:https://doi.org/10.1029/2000JD900839, 2001.
- 856Lopez-Hilfiker, F. D., Mohr, C., Ehn, M., Rubach, F., Kleist, E., Wildt, J., Mentel, T. F., Lutz, A.,
857 Hallquist, M., Worsnop, D. and Thornton, J. A.: A novel method for online analysis of gas and
858 particle composition: description and evaluation of a Filter Inlet for Gases and AEROSols
859 (FIGAERO), *J. Geophys. Res. Atmos.*, **7(4)**, 983–1001, doi:10.5194/amt-7-983-2014, 2014.
- 860Lopez-Hilfiker, F. D., Mohr, C., D'Ambro, E. L., Lutz, A., Riedel, T. P., Gaston, C. J., Iyer, S., Zhang, Z.,
861 Gold, A., Surratt, J. D., Lee, B. H., Kurten, T., Hu, W. W., Jimenez, J., Hallquist, M. and Thornton,
862 J. A.: Molecular Composition and Volatility of Organic Aerosol in the Southeastern U.S.:
863 Implications for IEPOX Derived SOA, *Environ. Sci. Technol.*, **50(5)**, 2200–2209,
864 doi:10.1021/acs.est.5b04769, 2016.
- 865Mao, J., Jacob, D. J., Evans, M. J., Olson, J. R., Ren, X., Brune, W. H., St. Clair, J. M., Crouse, J. D.,
866 Spencer, K. M., Beaver, M. R., Wennberg, P. O., Cubison, M. J., Jimenez, J. L., Fried, A.,
867 Weibring, P., Walega, J. G., Hall, S. R., Weinheimer, A. J., Cohen, R. C., Chen, G., Crawford, J.
868 H., McNaughton, C., Clarke, A. D., Jaeglé, L., Fisher, J. A., Yantosca, R. M., Le Sager, P. and
869 Carouge, C.: Chemistry of hydrogen oxide radicals (HOx) in the Arctic troposphere in spring,
870 *Atmos. Chem. Phys.*, **10(13)**, 5823–5838, doi:10.5194/acp-10-5823-2010, 2010.
- 871Mao, J., Paulot, F., Jacob, D. J., Cohen, R. C., Crouse, J. D., Wennberg, P. O., Keller, C. A., Hudman,
872 R. C., Barkley, M. P. and Horowitz, L. W.: Ozone and organic nitrates over the eastern United
873 States: Sensitivity to isoprene chemistry, *J. Geophys. Res. Atmos.*, **118(19)**, 11256–11268,
874 doi:10.1002/jgrd.50817, 2013.
- 875Martin, S. T., Artaxo, P., Machado, L. A. T., Manzi, A. O., Souza, R. A. F., Schumacher, C., Wang, J.,
876 Andreae, M. O., Barbosa, H. M. J., Fan, J., Fisch, G., Goldstein, A. H., Guenther, A., Jimenez, J.
877 L., Pöschl, U., Silva Dias, M. A., Smith, J. N. and Wendisch, M.: Introduction: Observations and
878 Modeling of the Green Ocean Amazon (GoAmazon2014/5), *Atmos. Chem. Phys.*, **16(8)**,
879 4785–4797, doi:10.5194/acp-16-4785-2016, 2016.
- 880Massoli, P., Stark, H., Canagaratna, M. R., Krechmer, J. E., Xu, L., Ng, N. L., Mauldin, R. L., Yan, C.,
881 Kimmel, J., Misztal, P. K., Jimenez, J. L., Jayne, J. T. and Worsnop, D. R.: Ambient
882 Measurements of Highly Oxidized Gas-Phase Molecules during the Southern Oxidant and
883 Aerosol Study (SOAS) 2013, *ACS Earth Sp. Chem.*, **2(7)**, 653–672,
884 doi:10.1021/acsearthspacechem.8b00028, 2018.
- 885McDonald, B. C., de Gouw, J. A., Gilman, J. B., Jathar, S. H., Akherati, A., Cappa, C. D., Jimenez, J.
886 L., Lee-Taylor, J., Hayes, P. L., McKeen, S. A., Cui, Y. Y., Kim, S.-W., Gentner, D. R.,
887 Isaacman-VanWertz, G., Goldstein, A. H., Harley, R. A., Frost, G. J., Roberts, J. M., Ryerson, T.
888 B. and Trainer, M.: Volatile chemical products emerging as largest petrochemical source of
889 urban organic emissions, *Science (80-.)*, **359(6377)**, 760–764, doi:10.1126/science.aaq0524,
890 2018.
- 891McFiggans, G., Mentel, T. F., Wildt, J., Pullinen, I., Kang, S., Kleist, E., Schmitt, S., Springer, M.,
892 Tillmann, R., Wu, C., Zhao, D., Hallquist, M., Faxon, C., Le Breton, M., Hallquist, A. M.,
893 Simpson, D., Bergstroem, R., Jenkin, M. E., Ehn, M., Thornton, J. A., Alfarra, M. R., Bannan, T.
894 J., Percival, C. J., Priestley, M., Topping, D. and Kiendler-Scharr, A.: Secondary organic aerosol
895 reduced by mixture of atmospheric vapours, *Nature*, **565(7741)**, 587–593,
896 doi:10.1038/s41586-018-0871-y, 2019.
- 897Mentel, T. F., Springer, M., Ehn, M., Kleist, E., Pullinen, I., Kurtén, T., Rissanen, M., Wahner, A. and
898 Wildt, J.: Formation of highly oxidized multifunctional compounds: autoxidation of peroxy



- 899 radicals formed in the ozonolysis of alkenes – deduced from structure–product relationships,
900 *Atmos. Chem. Phys.*, 15(12), 6745–6765, doi:10.5194/acp-15-6745-2015, 2015.
- 901 Messina, P., Lathièrre, J., Sindelarova, K., Vuichard, N., Granier, C., Ghattas, J., Cozic, A. and
902 Hauglustaine, D. A.: Global biogenic volatile organic compound emissions in the ORCHIDEE
903 and MEGAN models and sensitivity to key parameters, *Atmos. Chem. Phys.*, 16(22), 14169–
904 14202, doi:10.5194/acp-16-14169-2016, 2016.
- 905 Orlando, J. J., Tyndall, G. S. and Wallington, T. J.: The Atmospheric Chemistry of Alkoxy Radicals,
906 *Chem. Rev.*, 103(12), 4657–4690, doi:10.1021/cr020527p, 2003.
- 907 Palen, E. J., Allen, D. T., Pandis, S. N., Paulson, S. E., Seinfeld, J. H. and Flagan, R. C.: Fourier
908 transform infrared analysis of aerosol formed in the photo-oxidation of isoprene and
909 β -pinene, *Atmos. Environ. Part A. Gen. Top.*, 26(7), 1239–1251,
910 doi:https://doi.org/10.1016/0960-1686(92)90385-X, 1992.
- 911 Pandis, S. N., Harley, R. A., Cass, G. R. and Seinfeld, J. H.: Secondary organic aerosol formation
912 and transport, *Atmos. Environ. Part A. Gen. Top.*, 26(13), 2269–2282,
913 doi:https://doi.org/10.1016/0960-1686(92)90358-R, 1992.
- 914 Petaja, T., O'Connor, E. J., Moisseev, D., Sinclair, V. A. V. A., Manninen, A. J. A. J., Vaananen, R., von
915 Lerber, A., Thorntoton, J. A., Nicocoll, K., Petersen, W., Chandrasekar, V., Smith, J. N., Winkler,
916 P. M., Krueger, O., Hakola, H., Timonen, H., Brus, D., Laurila, T., Asmi, E., Riekkola, M.-L.,
917 Mona, L., Massoli, P., Engelmann, R., Kompppula, M., Wang, J., Kuang, C., Baeck, J., Virtanen,
918 A., Levula, J., Ritsche, M., Hickmon, N., Petäjä, T., O'Connor, E. J., Moisseev, D., Sinclair, V. A. V.
919 A., Manninen, A. J. A. J., Väänänen, R., von Lerber, A., Thornton, J. A., Nicoll, K., Petersen, W.,
920 Chandrasekar, V., Smith, J. N., Winkler, P. M., Krüger, O., Hakola, H., Timonen, H., Brus, D.,
921 Laurila, T., Asmi, E., Riekkola, M.-L., Mona, L., Massoli, P., Engelmann, R., Komppula, M.,
922 Wang, J., Kuang, C., Bäck, J., Virtanen, A., Levula, J., Ritsche, M. and Hickmon, N.: BAECC: A
923 Field Campaign to Elucidate the Impact of Biogenic Aerosols on Clouds and Climate, *Bull. Am.*
924 *Meteorol. Soc.*, 97(10), 1909–1928, doi:10.1175/BAMS-D-14-00199.1, 2016.
- 925 Pospisilova, V., Lopez-Hilfiker, F. D., Bell, D. M., El Haddad, I., Mohr, C., Huang, W., Heikkinen, L.,
926 Xiao, M., Dommen, J., Prevot, A. S. H., Baltensperger, U. and Slowik, J. G.: On the fate of
927 oxygenated organic molecules in atmospheric aerosol particles, *Sci. Adv.*, 6(11),
928 doi:10.1126/sciadv.aax8922, 2020.
- 929 Richters, S., Herrmann, H. and Berndt, T.: Highly Oxidized RO₂ Radicals and Consecutive Products
930 from the Ozonolysis of Three Sesquiterpenes, *Environ. Sci. & Technol.*, 50(5), 2354–2362,
931 doi:10.1021/acs.est.5b05321, 2016.
- 932 de Sa, S. S., Palm, B. B., Campuzano-Jost, P., Day, D. A., Hu, W., Isaacman-VanWertz, G., Yee, L. D.,
933 Brito, J., Carbone, S., Ribeiro, I. O., Cirino, G. G., Liu, Y., Thalman, R., Sedlacek, A., Funk, A.,
934 Schumacher, C., Shilling, J. E., Schneider, J., Artaxo, P., Goldstein, A. H., Souza, R. A. F., Wang,
935 J., McKinney, K. A., Barbosa, H., Alexander, M. L., Jimenez, J. L. and Martin, S. T.: Urban
936 influence on the concentration and composition of submicron particulate matter in central
937 Amazonia, *Atmos. Chem. Phys.*, 18(16), 12185–12206, doi:10.5194/acp-18-12185-2018,
938 2018.
- 939 Travis, K. R., Jacob, D. J., Fisher, J. A., Kim, P. S., Marais, E. A., Zhu, L., Yu, K., Miller, C. C., Yantosca,
940 R. M., Sulprizio, M. P., Thompson, A. M., Wennberg, P. O., Crouse, J. D., St Clair, J. M., Cohen,
941 R. C., Laughner, J. L., Dibb, J. E., Hall, S. R., Ullmann, K., Wolfe, G. M., Pollack, I. B., Peischl, J.,
942 Neuman, J. A. and Zhou, X.: Why do models overestimate surface ozone in the Southeast



- 943 United States?, *Atmos. Chem. Phys.*, 16(21), 13561–13577, doi:10.5194/acp-16-13561-2016,
944 2016.
- 945 Wang, J., Krejci, R., Giangrandel, S., Kuang, C., Barbosa, H. M. J., Brito, J., Carbone, S., Chi, X.,
946 Comstock, J., Ditas, F., Lavric, J., Manninen, H. E., Mei, F., Moran-Zuloaga, D., Poehlker, C.,
947 Poehlker, M. L., Saturno, J., Schmid, B., Souza, R. A. F., Springston, S. R., Tomlinson, J. M., Toto,
948 T., Walter, D., Wimmer, D., Smith, J. N., Kulmala, M., Machado, L. A. T., Artaxo, P., Andreae, M.
949 O., Petaja, T. and Martin, S. T.: Amazon boundary layer aerosol concentration sustained by
950 vertical transport during rainfall, *Nature*, 539(7629), 416–419, doi:10.1038/nature19819,
951 2016.
- 952 Weber, J., Archer-Nicholls, S., Griffiths, P., Berndt, T., Jenkin, M., Gordon, H., Knote, C. and
953 Archibald, A. T.: CRI-HOM: A novel chemical mechanism for simulating highly oxygenated
954 organic molecules (HOMs) in global chemistry–aerosol–climate models, *Atmos. Chem. Phys.*,
955 20(18), 10889–10910, doi:10.5194/acp-20-10889-2020, 2020.
- 956 Wesely, M. L.: Parameterization of surface resistances to gaseous dry deposition in regional-scale
957 numerical models, *Atmos. Environ.*, 23(6), 1293–1304,
958 doi:https://doi.org/10.1016/0004-6981(89)90153-4, 1989.
- 959 Xu, L., Pye, H. O. T., He, J., Chen, Y., Murphy, B. N. and Ng, N. L.: Experimental and model
960 estimates of the contributions from biogenic monoterpenes and sesquiterpenes to
961 secondary organic aerosol in the southeastern United States, *Atmos. Chem. Phys.*, 18(17),
962 12613–12637, doi:10.5194/acp-18-12613-2018, 2018.
- 963 Xu, L., Møller, K. H., Crouse, J. D., Otkjær, R. V., Kjaergaard, H. G. and Wennberg, P. O.:
964 Unimolecular reactions of peroxy radicals formed in the oxidation of α -Pinene and β -Pinene
965 by hydroxyl radicals, *J. Phys. Chem. A*, doi:10.1021/acs.jpca.8b11726, 2019.
- 966 Zawadowicz, M. A., Lee, B. H., Shrivastava, M., Zelenyuk, A., Zaveri, R. A., Flynn, C., Thornton, J. A.
967 and Shilling, J. E.: Photolysis Controls Atmospheric Budgets of Biogenic Secondary Organic
968 Aerosol, *Environ. Sci. & Technol.*, 54(7), 3861–3870, doi:10.1021/acs.est.9b07051, 2020.
- 969 Zhang, H., Yee, L. D., Lee, B. H., Curtis, M. P., Worton, D. R., Isaacman-VanWertz, G., Offenberg, J.
970 H., Lewandowski, M., Kleindienst, T. E., Beaver, M. R., Holder, A. L., Lonneman, W. A.,
971 Docherty, K. S., Jaoui, M., Pye, H. O. T., Hu, W., Day, D. A., Campuzano-Jost, P., Jimenez, J. L.,
972 Guo, H., Weber, R. J., de Gouw, J., Koss, A. R., Edgerton, E. S., Brune, W., Mohr, C.,
973 Lopez-Hilfiker, F. D., Lutz, A., Kreisberg, N. M., Spielman, S. R., Hering, S. V., Wilson, K. R.,
974 Thornton, J. A. and Goldstein, A. H.: Monoterpenes are the largest source of summertime
975 organic aerosol in the southeastern United States, *Proc. Natl. Acad. Sci. U. S. A.*, 115(9),
976 2038–2043, doi:10.1073/pnas.1717513115, 2018.
- 977 Zhang, L., Gong, S., Padro, J. and Barrie, L.: A size-segregated particle dry deposition scheme for
978 an atmospheric aerosol module, *Atmos. Environ.*, 35(3), 549–560,
979 doi:https://doi.org/10.1016/S1352-2310(00)00326-5, 2001.
- 980 Zhang, S.-H., Shaw, M., Seinfeld, J. H. and Flagan, R. C.: Photochemical aerosol formation from
981 α -pinene- and β -pinene, *J. Geophys. Res. Atmos.*, 97(D18), 20717–20729,
982 doi:https://doi.org/10.1029/92JD02156, 1992.
- 983 Zhao, B., Shrivastava, M., Donahue, N. M., Gordon, H., Schervish, M., Shilling, J. E., Zaveri, R. A.,
984 Wang, J., Andreae, M. O., Zhao, C., Gaudet, B., Liu, Y., Fan, J. and Fast, J. D.: High
985 concentration of ultrafine particles in the Amazon free troposphere produced by organic new
986 particle formation, *Proc. Natl. Acad. Sci.*, 117(41), 25344–25351,



987 doi:10.1073/pnas.2006716117, 2020.
988 Zhao, Y., Thornton, J. A. and Pye, H. O. T.: Quantitative constraints on autoxidation and dimer
989 formation from direct probing of monoterpene-derived peroxy radical chemistry, Proc. Natl.
990 Acad. Sci. U. S. A., 115(48), 12142–12147, doi:10.1073/pnas.1812147115, 2018.
991